Influence of tissue optical properties on laser Doppler perfusion imaging, accounting for photon penetration depth and the laser speckle phenomenon

Vinayakrishnan Rajan
Babu Varghese
Ton G. Van Leeuwen
Wiendelt Steenbergen
University of Twente
Institute for Biomedical Technology
Biophysical Engineering Group
P.O Box 217
NL-7500AE Enschede, The Netherlands
E-mail: v.rajan@tnw.utwente.nl

Abstract. The influence of tissue optical properties on laser Doppler perfusion imaging (LDPI) is not well understood. We address this problem by quantifying the dependence of the signal response to tissue optical properties based on speckles or coherence areas and on photon statistics. We investigate the effect *in vivo*, showing the amplitude of photocurrent fluctuations in normal skin and port-wine stain with a range of beam diameters, and its relation to the speckle size variation difference between these two tissues. For the case of a low concentration of moving particles moving within a static turbid medium, a model is described and applied to predict the influence of speckles on the overall and depth sensitivity of LDPI, for a range of scattering levels and absorption levels. The results show that the speckle related effects on overall and depth sensitivity are large and that the depth sensitivity is highly likely to be misinterpreted without taking the speckle phenomenon into account. [DOI: 10.1117/1.2904958]

Keywords: laser Doppler perfusion imaging; coherence area; depth sensitivity; tissue optical properties; sampling depth; Monte Carlo simulations.

Paper 07262 received Jul. 18, 2007; accepted for publication Nov. 27, 2007; published online Apr. 8, 2008.

1 Introduction

Coherence domain optical methods used for tissue perfusion imaging[1–5] are based on the analysis of dynamic speckles formed by the light backscattered from the tissue.[6] Laser Doppler perfusion imaging (LDPI) is such a technique and is based on the analysis of spatial and temporal variation of speckles due to the motion of moving blood cells in the microcirculation.[3,4] Recently, we showed that independent of the perfusion, the LDPI response is influenced by speckles.[7] The modulation depth of the photodetector signal depends on the speckles and thus beam diameter. We showed that with a typical beam diameter of 0.5 mm the average speckle size on the detector varies by a factor of 4 when the reduced scattering level varied from 0.5 to 4.0 mm^{-1}. This variation drops to a factor of 1.5 when the beam diameter is increased to 4.0 mm, which demonstrates the interplay between the speckle size and perfusion signal on the LDPI response due to the fact that the speckle size is inversely related to the width of the intensity distribution.

The perfusion in a region where the optical properties are either spatially heterogeneous or change in time can be erroneously estimated. For example during a vasodilatory stimulus,[8] the tissue optical properties change, resulting in intensity distribution variations of the reflected light in course of time. In the case of burn diagnosis,[9] the heterogeneous nature of the burn tissue and presence of inflammation can influence the perfusion map, since the scanning beam will go through areas where either absorption or scattering is different. This will result in different widths of backscattered intensity distributions and different solid angles of illumination on the far-field detector (Fig. 1). The speckle size and number will vary in time and with the location on the tissue with optical properties, causing variations in the perfusion reading independent of actual perfusion variations. Thus, it is very important that the issue of speckles is quantified in these cases.

We have reported that the spatial correlations of the intensity of far-field dynamic speckle patterns generated by mixed static and dynamic turbid media illuminated by coherent light can be predicted.[10] Based on a theoretical/computational framework, the variance of photocurrent fluctuations was modeled for a far-field detector collecting backscattered photons on the basis of Monte-Carlo-derived photon statistics, taking into account the speckle phenomenon. The speckle size variations were estimated for different scattering levels and anisotropies.

In this paper, first we demonstrate the influence of tissue optical properties on the signal response as mediated by the speckle effect *in vivo* by comparing the signal from normal skin and port-wine-stained skin for various beam diameters. Next, we use our validated computational method to quantify the overall sensitivity and depth-resolved response of LDPI due to the combined effect of photon penetration depth statis-

Address all correspondence to Vinayakrishnan Rajan, Biophysical Engineering Group, University of Twente, Building 28 - Enschede, Overijssel 7523TW Netherlands; Tel: 0031534891080; Fax: 0031 534891105; E-mail: v.rajan@tnw.utwente.nl

1083-3668/2008/13(2)/024001/9/$25.00 © 2008 SPIE

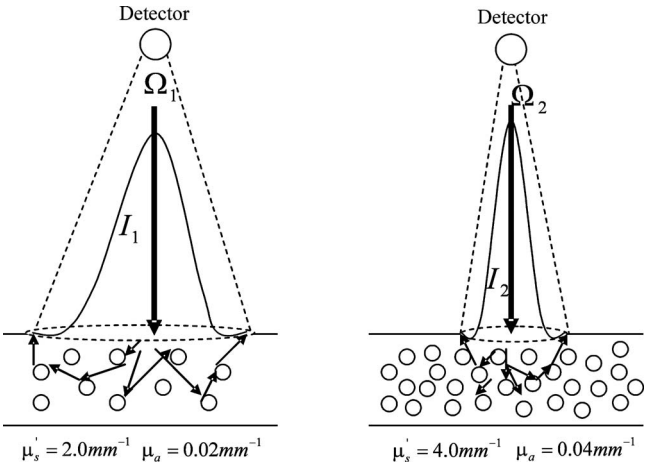

Fig. 1 Intensity profile and the solid angle generated by the backscattered photons for two different optical properties; I_1 and I_2 represents the intensity distributions and Ω_1 and Ω_2 represents the solid angles.

tics and the speckle phenomenon. This is done for a range of tissue optical properties.

2 Theoretical Background

In the laser Doppler perfusion measurement technique, information about the amount and flux of the moving scatterers (red blood cells) are extracted from the power spectra of photocurrent intensity fluctuations.[11] The moments of the power spectra give an estimation of perfusion,

$$M_i = \int_0^\infty P(\omega)\omega^i \, \mathrm{d}\omega, \tag{1}$$

often normalized with dc^2 to cancel out laser power fluctuations. The first moment M_1 is regarded as a measure of the flux of the moving scatterers (also called the perfusion) and M_0, the zero-order moment, is considered to represent the concentration of moving scatterers.

2.1 *LDPI Signal Modulation Depth*

In LDPI the moments of the power spectrum of the detector current fluctuations depend on the spectral width and the modulation depth of the signal. The latter quantity in turn is related to the amount of speckles within the photodetector area. The zero-order moment normalized with the dc^2 signal can be written as[10]

$$\tilde{M} \equiv \frac{M_0}{\mathrm{dc}^2} \equiv \frac{\langle i_{\mathrm{ac}}^2 \rangle}{\langle i_{\mathrm{dc}} \rangle^2} = \frac{2\sum_i^M f_0 f_i A_{\mathrm{coh}}^{0i} + \sum_{i=1}^M \sum_{j=1}^M f_i f_j A_{\mathrm{coh}}^{ij}}{A_{\mathrm{det}}}, \tag{2}$$

where $\langle i_{\mathrm{ac}}^2 \rangle$ is the mean square of the photocurrent fluctuations, $\langle i_{\mathrm{dc}} \rangle$ is the mean photocurrent, and A_{det} is the effective detection area (in the case of light collection with a lens, the area of the lens is the effective detection area). Furthermore f_0 is the fraction of non-Doppler-shifted photons, while $f_1, \ldots, f_m$ represent fractions of Doppler-shifted photons that can be defined on the basis of various criteria, such as the Doppler shift, the number of Doppler scattering events, the (optical) path length, and the penetration depth into the medium. Also, A_{coh}^{ij} represents the so-called fractional coherence area on the detector formed by all pairs of photon groups i and j. These fractional coherence areas can be written in terms of respective correlation functions as

$$A_{\mathrm{coh}}^{ij} = 2\pi \int_0^\infty \gamma_{\mathrm{EE}}^{j}(\Delta x)\gamma_{\mathrm{EE}}^{*j}(\Delta x)\Delta x \, \mathrm{d}\Delta x. \tag{3}$$

Here i and $j=0$, 1, represent non-Doppler-shifted light and Doppler-shifted light, respectively, and γ_{EE} represents the field correlation function of the waves of Doppler shifted and unshifted light that illuminate the photodetector. The field correlation function for each fraction of light can be written in terms of the intensity distribution using the Zernike-van Cittert theorem,

$$\gamma_{\mathrm{EE}}(\Delta X, \Delta Y) = \frac{\int\int_{\mathrm{source}} I(x,y) \exp\left[-i(2\pi/\lambda Z)(x\Delta X + y\Delta Y)\right] \mathrm{d}x \, \mathrm{d}y}{\int\int_{\mathrm{source}} I(x,y) \, \mathrm{d}x \, \mathrm{d}y}, \tag{4}$$

where $I(x,y)$ is the intensity distribution on the surface of the medium with x, y, ΔX, and ΔY the positions on the surface of the turbid medium, and spatial separations on the plane of detection, respectively; Z is the distance of the medium to the detector plane; and λ is the wavelength of light in the transparent medium between the turbid medium and the detector.

Since the Monte Carlo method[12] can simulate the photon intensity distribution from an optical medium and provide the statistics of fractions of Doppler-shifted photons, it can give input parameters to calculate the fractional coherence areas on the photodetector, and in turn we can predict the signal modulation depth.

2.2 *Depth Sensitivity Prediction in LDPI*

The depth sensitivity of LDPI can be defined as the sensitivity of the instrument to motion of red blood cells at a certain depth under the tissue surface. Our initial approach is to analyze this quantity for a static medium with a relatively low concentration of moving scatterers. In that case, the modulation depth can be predicted for two fractions of photons; one that has interacted only with the static medium and is non-Doppler shifted and one that interacted with the particles moving at a certain depth and is Doppler shifted. In this case, we can write Eq. (2) as

$$\tilde{M} \equiv \frac{M_0}{\mathrm{dc}^2} \equiv \frac{\langle i_{ac}^2 \rangle}{\langle i_{\mathrm{dc}} \rangle^2} = \frac{[2f_0 f_1 A_{\mathrm{coh}}^{01} + f_1^2 A_{\mathrm{coh}}^{11}]}{2A_{\mathrm{det}}}, \tag{5}$$

where f_0 is the fraction of non-Doppler-shifted photons, f_1 is the fraction of Doppler-shifted photons, A_{coh}^{01} is the coherence area formed by the interference of Doppler-shifted photons with non-Doppler-shifted photons, and A_{coh}^{11} is the fraction of coherence area formed by only Doppler shifted photons. Here a factor of 2 is introduced in the denominator, since a nonpo-

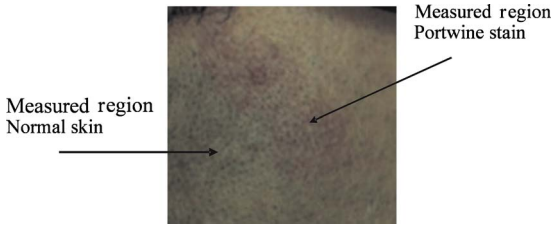

Fig. 2 Photograph of the measured port-wine stain on the right cheek of the subject.

larized speckle pattern is a summation of two independent orthogonally polarized patterns that are formed by multiple scattering. The first term of the numerator of Eq. (5) represents the heterodyne signal formed by the interference of Doppler-shifted light with non-Doppler-shifted light. The other part represents the homodyne signal that is formed by the interference of only Doppler shifted light.

In tissue that is sparsely perfused the Doppler shifted fraction of photons will be significantly smaller than the non-Doppler-shifted photons, and hence $f_1^2 \ll f_0 f_1$. In that case, the contribution from the homodyne part of the signal [the second term in the numerator of Eq. (5)] will be negligible and Eq. (5) assumes a more simplified form:

$$\tilde{M} \equiv \frac{M_0}{\mathrm{dc}^2} \equiv \frac{\langle i_{\mathrm{ac}}^2 \rangle}{\langle i_{\mathrm{dc}} \rangle^2} = f_0 f_1 \frac{A_{\mathrm{coh}}^{01}}{A_{\mathrm{det}}}. \tag{6}$$

3 Materials and Methods

In this section, we describe the methods we followed to give *in vivo* evidence of the independent effect of speckles on the response of LDPI. Next, we analyze the influence of tissue optical properties on LDPI signal, with incorporation of speckle effects. We performed measurements on two skin sites to analyze the LDPI signal differences and to correlate this with the speckle size predicted on the basis of the measured intensity distribution. A relation between the measured perfusion levels, the optical properties, and the speckle phenomenon is also suggested by a concise Monte Carlo study. Finally, having given proof of the relevance of the speckle effect *in vivo*, we performed a series of simulations with various optical properties.

3.1 *In Vivo Measurements*

The aim of the *in vivo* measurements was to confirm the effect of speckles on perfusion measurements in real tissue. For this, we measured on and next to a port-wine stain in the face of a human subject. Since the port-wine stain has an abnormal density of blood vessels, the optical properties will be significantly different from the surrounding normal skin.

The port-wine stain we measured was on the right cheek of a healthy subject (male, 42 years old) and was pale red in color. Figure 2 is a photograph of the measured region of the cheek with port-wine stain. A photoacoustic image of the cheek skin was obtained, with a setup available in our group[13] to analyze the thickness and depth of the port-wine stain region. The thickness of the port-wine stain was measured to be 2 mm and the depth of the lesion under the skin surface was estimated as 300 μm. Since the penetration depth of the laser Doppler imager setup is around 1 mm (depends on the tissue optical properties), the probed tissue volume was completely inside the boundaries of the highly vascularized region.

3.1.1 *Experimental setup for laser Doppler measurements*

The experimental setup consisted of a simple backscattered configuration in which we illuminated the skin with a perpendicular laser beam and collected the backscattered light using a lens and a photoreceiver. A linearly polarized 632.8-nm Uniphase 1125P He-Ne laser with an output power of 5 mW was used as the source. A beam expander made of two positive lenses of focal lengths 20 and 30 mm, respectively, was used to vary the beam diameter. The beam diameter was measured with a commercial beam profiler. A 11-mm-diam lens (f =30 mm) was placed at a distance of 25 cm from the sample to collect the backscattered light, with a photoreceiver in focus (New Focus, model 2001) with a detector area of 0.81 mm^2. The ac signal was amplified by 40 dB and then applied to an antialiasing low-pass filter (fifth-order sampled capacitor Butterworth, f_c=20 kHz). The filtered signal was then applied to a 12-bit analog-to-digital converter, where it was sampled at 40 kHz. The power spectrum of this ac signal was used to calculate the normalized zero-order moment M_0/dc^2. The M_0/dc^2 signal was measured using a range of beam diameters and measurements were compared between normal skin (adjacent to the stain) and the port-wine-stained skin. In all cases, only one-point measurements were taken, with averaging over three measurements.

3.1.2 *Average speckle size measurement*

We showed earlier that the average speckle size produced on a far-field detector by light backscattered from a scattering medium can be calculated using the intensity distribution of back scattered light.[11] To measure the backscattered intensity distribution from the normal skin and port wine stain we used a CMOS camera (C-Cam, Bci4-USB). The correlation function and the speckle size were calculated from this intensity profile with the procedure explained in Sec. 2.1. For simplicity, it was assumed that there was only one fraction of photons, since it is not possible to discriminate between fractions of photons according to the depth or Doppler shift in real tissue. This gives the average speckle size [coherence area, see Eq. (3)] related to the measured intensity distribution.

3.2 *Monte Carlo Simulations*

In the Monte Carlo simulation the scattering phantom was defined as a 2-D layered system containing particles of diameter $\varnothing$0.771 μm (scattering anisotropy g=0.89). A 632.8-nm collimated Gaussian beam with different beam diameters was used as the source and was positioned perpendicular to the interface of the medium. In Monte Carlo simulation, a 50-mm-radius circular detector was used, which is sufficient enough to collect all the backscattered photons. Each simulation was carried out with a fixed number of detected photons (90,000).

Table 1 Optical properties and depth of moving layer for the Monte Carlo simulation.

μ_s' (mm^{-1})	1.0	2.0	3.0	4.0			
μ_a' (mm^{-1})	0.01	0.02	0.04	0.08			
g	0.89						
Depths of dynamic layer (mm)	0	0.25	0.5	0.75	1.0	1.5	2.0

3.2.1 *Influence of beam diameter on modulation depth*

To validate our observations in *in vivo* measurements, we used our model to calculate the modulation depth for two optical situations resembling to normal skin and port-wine stain. Since the optical properties of the port-wine stain and the adjacent skin we measured on are not known, we assumed a higher scattering and very high absorption compared to normal skin.[14] For this, one medium was defined with scattering and absorbing levels of $\mu_s'=2.0$ mm^{-1} and $\mu_a=0.02$ mm^{-1} and another medium with $\mu_s'=4.0$ mm^{-1} and $\mu_a=0.04$ mm^{-1} to mimic the variation in optical properties of the normal skin and the port-wine stain, respectively. A series of simulations were performed by varying the $1/e^2$ beam diameter as 0.5, 1.0, 1.5, 2.0, 3.0, and 4.0 mm.

In each simulation, the intensity distribution of all detected photons (not discriminating the depth) was used in calculating the average speckle size by Eqs. (3) and (4). Next, using Eq. (5), the overall response of the signal in terms of its modulation depth was calculated assuming $f_0=0$ and $f_1=1$. This gives an overall response of the signal for different tissue optical properties and beam diameters.

3.2.2 *Influence of tissue optical properties on the depth sensitivity*

To quantify the influence of tissue optical properties on depth sensitivity we considered motion of a low concentration of scattering particles in a static medium, and we analyzed the signal modulation depth generated by particles confined within a thin layer at a certain depth. This was repeated for a number of depths of the thin dynamic layer in the range 0 to 2 mm, and for different combinations of tissue optical properties as given in Table 1. The scattering medium was illuminated with a Gaussian beam of a $1/e^2$ beam diameter of 1 mm. Since this beam diameter is typical for commercially available laser Doppler imagers the results will be very useful for analyzing the performance of the method. The refractive index of the medium containing the scattering particles and the surrounding medium were defined as 1.33 and 1, respectively. A series of simulations were performed with all combinations of optical properties defined in Table 1.

For each simulation, the intensity distributions of Doppler-shifted and -unshifted photons were determined. This discrimination was done by separating the photons with maximum penetration depth exceeding the depth of the assumed moving layer (leading to fraction f_1) from photons with a maximum depth upto the depth of the moving layer (leading to fraction f_0). In designing this procedure, the key reasoning was that motion in a thin layer at a certain depth can only be detected by light reaching at least that specific depth. While the relative amount of photons that will be Doppler shifted by motion in thin layers at the various depths is regarded as proportional to the relative amount f_1 of photons reaching at least these depths, the absolute amount of photons Doppler shifted by a certain thin moving layer would also depend on the assumed thickness of the moving layer, the concentration of particles moving within this layer and the number of times that an eventually detected photon will cross this layer. The latter quantity is assumed to be only a weak function of the optical properties, and to be only weakly depth dependent. And as long the first two quantities are not specified, f_1 as a function of depth is a measure for the relative sensitivity to motion at a certain depth.

To determine the contribution of the motion at a certain depth to the modulation depth of the signal Eq. (6) is used. The coherence area A_{coh}^{01} is calculated by Eq. (3) using the field correlation functions obtained with the intensity distribution of the statically scattered photons and dynamically scattered photons by Eq. (4). Considering the optical situation of tissue that is sparsely seeded with dynamic scatterers (mimicking sparsely perfused tissue) we assume a constant intensity distribution for the fraction f_0 of non-Doppler-shifted photons and a depth dependent intensity distribution of the fraction f_1 of Doppler-shifted photons in calculating A_{coh}^{01}. This fixed intensity distribution of nonshifted light is taken as equal to the intensity distribution of all photons being diffusely reflected from the medium. Furthermore, we assumed the fraction f_0 of nonshifted photons to be independent of the depth at which motion is assumed. For sparsely dynamic media, this is a realistic assumption, since the real relative variation of f_0, which is close to 1 in all cases, is much smaller than the relative variation of f_1, which ranges from 0 for motion at large depth, to a maximum value for motion at depth. The consequence of this approach is that Eq. (6) is reduced to

$$\tilde{M} \equiv \frac{M_0}{\mathrm{dc}^2} \equiv \frac{\langle i_{\mathrm{ac}}^2 \rangle}{\langle i_{\mathrm{dc}} \rangle^2} = \beta f_1 A_{\mathrm{coh}}^{01}, \tag{7}$$

with β depending on the thickness of the thin moving layers, the concentration of moving scattering particles, and the effective detector area.

3.2.3 *Overall sensitivity and mean sampling depth*

The overall sensitivity is defined as the modulation depth of the instrument for simultaneous motion at all possible depths. This can be calculated from the modulation depth distribution for motion at various depths. If $\tilde{M}(x)$ is the calculated modulation depth generated by motion at a certain depth x, the overall sensitivity is given by $\int_{x_0}^{\infty} \tilde{M}(x)(x)\,\mathrm{d}x$, with x_0 the zero depth. This simple summation of sensitivities is allowed as long as the condition $f_1^2 \ll f_0 f_1$ holds, even when there is motion at all depths at the same time.

The mean sampling depth is defined as the weighted function of the overall depth sensitivity given by,

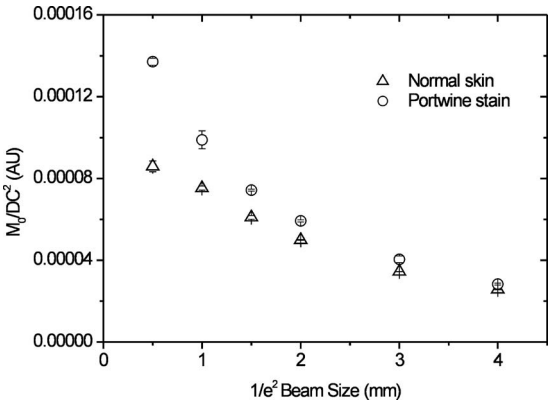

Fig. 3 Values of M_0/dc^2 as a function of beam diameter for normal skin and port-wine stain.

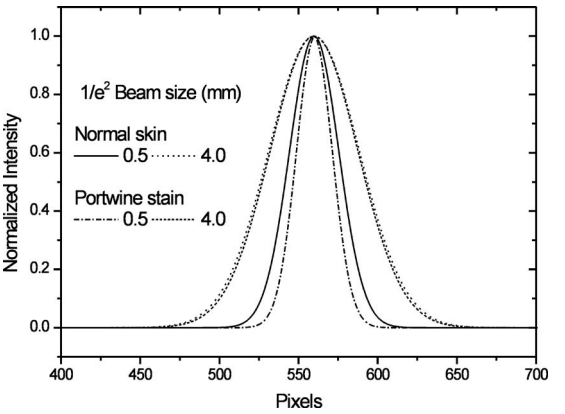

Fig. 4 Backscattered intensity distribution obtained with CMOS sensor from normal skin and port-wine stain. The raw intensity distribution is Gaussian fitted and normalized.

$$\text{mean sampling depth} = \frac{\int_{x_0}^{\infty} x\tilde{M}(x)\,\mathrm{d}x}{\int_{x_0}^{\infty} \tilde{M}(x)\,\mathrm{d}x}. \tag{8}$$

The mean sampling depth function gives the average depth probed by the photons for various optical properties. The average sensitivity and mean sampling depth were calculated for all optical properties given in Table 1. This was done for plots with Eq. (6) where the speckle phenomenon is considered and without speckle phenomenon by putting $A_{\mathrm{coh}}^{01}=1$ in Eq. (7) in calculating the modulation depth.

4 Results and Discussion

4.1 *In Vivo Measurements*

Figure 3 shows measured values of M_0/dc^2 (modulation depth) with different beam diameters for one position on the port-wine stain and one position on the surrounding normal skin. It can be observed that for normal skin and port-wine-stained skin the modulation depth decreases with increasing beam diameter. This change of decreasing modulation depth with beam diameter is larger for port-wine-stained skin than for normal skin. On the port-wine-stained region, increasing the beam diameter from 0.5 to 4.0 mm results in a decrease in modulation depth by a factor of 4.8, whereas for a normal skin, this decrease is only a factor of 3.3. Another observation is that for increasing beam diameter, the signal modulation depth for both skin locations converge.

4.2 *Average Speckle Size Measurement*

The intensity distributions measured with the CMOS camera for two skin types for a narrow beam and a wide beam are plotted in Fig. 4. The raw intensity distribution is Gaussian fitted and normalized. The plot shows a clear difference in intensity width for the narrow beam in the two skin types, while for a wide beam there is no significant difference. The speckle areas as calculated on the basis of the measured intensity distributions in the port-wine stain and the adjacent normal skin are shown in Fig. 5.

For a narrow beam (0.5 mm) the speckle size in a normal skin is a factor of 1.9 less compared to that in a port-wine stain. The effect of that can be seen in the measured modulation depth M_0/dc^2, where for 0.5 mm, there is a factor of 1.6 difference between normal skin and port-wine-stained skin. For a wide beam, however, the average speckle size difference is only by a factor of 1.1, which is also reflected in the measured M_0/dc^2 for this beam diameter.

A port-wine stain contains an abnormal density of blood vessels, which results in higher absorption and scattering by red blood cells compared to normal skin.[14] This leads to a narrow backscattered intensity distribution and a smaller number of speckles on the detector compared to normal skin. In experiments with a narrow laser beam, the obtained signal amplitudes will be very sensitive to this intensity width variation with tissue type. On the other hand, for a wide beam, which itself generates a wide intensity distribution and a large number of speckles, the speckle number variation with tissue types is suppressed. For beam diameters of 3 mm and larger, this leads to almost identical speckle areas and signal modulation depths.

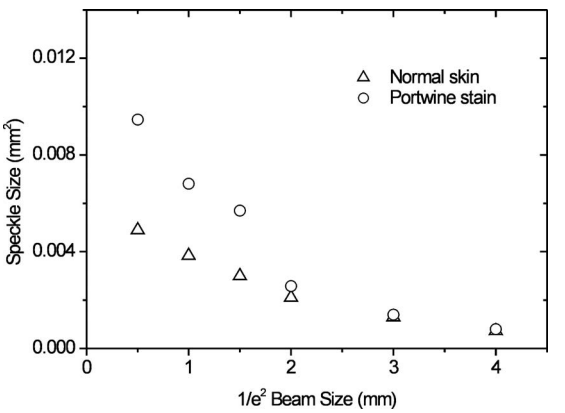

Fig. 5 Average speckle size calculated from the measured intensity distributions for normal skin and port-wine stain.

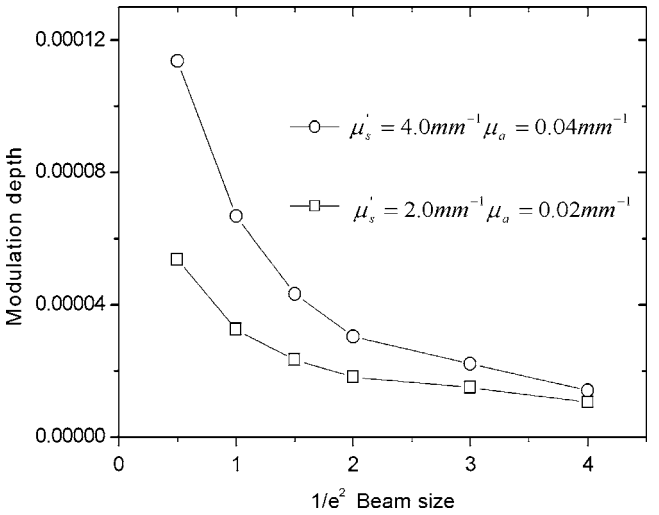

Fig. 6 Modulation depth versus beam diameter for two scattering mediums μ_s'=2.0 mm^{-1} and μ_a=0.02 mm^{-1} and μ_s'=4.0 mm^{-1} and μ_a =0.04 mm^{-1}.

4.3 *Influence of Beam Diameter and Tissue Optical Properties on Modulation Depth*

Figure 6 shows the modulation depth for different beam diameters calculated with Monte Carlo simulations, for simulated tissues representing normal and port-wine-stained skin. It can be seen that the modulation depth decreases with beam diameter for the two scattering mediums. However, when the reduced scattering level and absorption are increased from μ_s'=2.0 mm^{-1} and μ_a=0.02 mm^{-1} to μ_s'=4.0 mm^{-1} and μ_a=0.04 mm^{-1}, mimicking the transition from normal skin to the port-wine stain, the decrease in modulation depth with beam diameter increases from a factor of 5 to 8. This supports our observation of a larger influence of speckles in a port-wine stain, which has a higher scattering and absorption level compared to normal skin. For a narrow beam, this influence is significant, whereas for a wide beam this effect is suppressed.

4.4 *Influence of Tissue Optical Properties on the Depth Sensitivity*

The depth sensitivity, which is defined here as the modulation depth of the photodetector signal generated by particle motion at a certain depth under the surface of the static medium, was studied computationally. Figures 7(a)–7(d) show the modulation depth for various scattering levels as a function of the depth at which motion occurs, considering all the combinations of scattering levels, absorption levels, and depths given in Table 1. It is clear from the graph that the modulation depth drops with motion depth, which is more pronounced for higher scattering levels for a particular absorption level. It can be observed that in Fig. 7(a) for a scattering level of μ_s' =4.0 mm^{-1} and μ_a=0.01 mm^{-1}, the sensitivity for motion at largest depth decreases by an order of magnitude (factor of 50). The relative suppression of deep photons is reduced for decreasing scattering levels. For a scattering level of μ_s' =1.0 mm^{-1}, this decrease is only by a factor of 8.7. This recovery is stronger for increasing absorption. In Fig. 7(d) for μ_a=0.08 mm^{-1}, the sensitivity at larger depth for μ_s' =4.0 mm^{-1} is reduced by two orders of magnitude (factor of

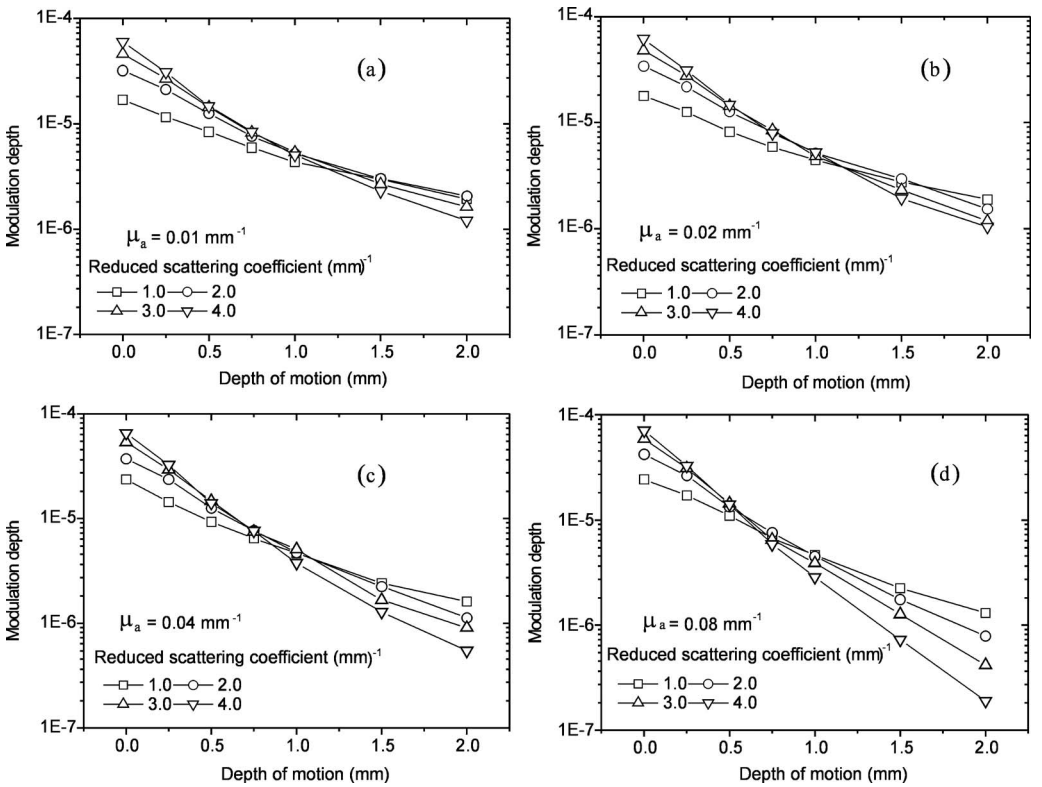

Fig. 7 (a) to (d) Modulation depth as a function of the assumed depth of motion and scattering and absorption levels.

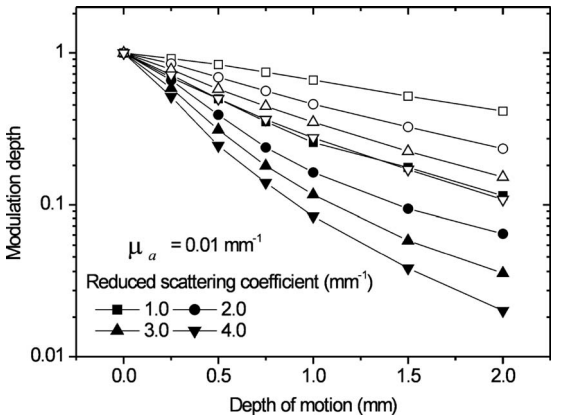

Fig. 8 Modulation depth (normalized to zero depth) versus depth of motion with speckle effects (shaded symbols) and without the speckle effects (closed symbols, $A_{coh}^{01}=1$) for $\mu_a=0.01$ mm^{-1}.

373), whereas for $\mu_s'=1.0$ mm^{-1} it is reduced by a factor of only 19. This trend is a combination of speckle effects and the changes in the photon penetration depth with optical properties.

The modulation depth (normalized to zero depth) versus depth of motion for $\mu_a=0.01$ mm^{-1} with speckle effects (shaded symbols) and without taking speckle effects [closed symbols, by keeping $A_{coh}^{01}=1$ in Eq. (7)] into account is shown as Fig. 8. The closed symbols depict the data of Fig. 7(a) without speckle effects, thus the modulation depth is a function of only the fraction of Doppler shifted photons. Consequently, the sensitivity for motion at zero depth is equal for all scattering levels, since all detected photons will cross this level. Figure 8 shows that for a scattering level of $\mu_s'=4.0$ mm^{-1} ignoring the speckle effects leads to a 10-fold decrease in sensitivity for motion at largest depth, while including the speckle phenomenon leads to a 50-fold decrease. For the lowest scattering level ($\mu_s'=1.0$ mm^{-1}) excluding the speckle effect leads to a less pronounced decrease in depth sensitivity (8.7 versus 2.5).

This trend of speckle effects on the modulation depth with varying scattering and absorption levels can be explained as follows. The deeper the light travels, the wider the intensity distribution will be and the smaller the speckles, resulting in an increase in the number of speckles with scattering depth. This increase results in a decreasing modulation depth. In the case of a higher absorption or scattering medium, the backscattered total intensity distribution will be narrow and the number of speckles will be less. Thus, in this case, the variation in the intensity width (and number of speckles) with variation in depth of motion of photons will be more sensitive. Thus, the speckle effect will be higher in this case compared to the situation where lower scattering and absorption levels generate a wide distribution of intensity and a large number of speckles.

4.5 *Overall Sensitivity and Sampling Depth*

The overall sensitivity, which for the sparsely perfused medium is the summation of the sensitivities for motion at all separate depths [see Eq. (8)], is presented in Fig. 9(a), which shows that the sensitivity increases with increasing scattering

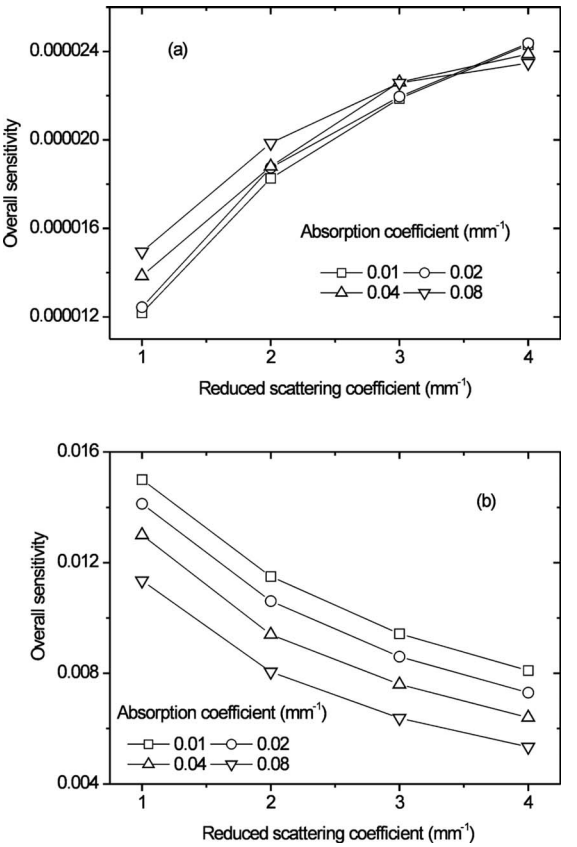

Fig. 9 Overall depth sensitivity for various optical properties (a) with the speckle phenomenon and (b) without taking the speckle phenomenon into consideration ($A_{coh}^{01}=1$).

and absorption levels. An increase of sensitivity with absorption seems contradictory. However, it can be understood from the speckle phenomenon. Both an increase in scattering and an increase in absorption result in a more narrow intensity distribution of backscattered light, and therefore lead to larger speckles. At higher scattering levels, the absorption has less influence on sensitivity than at lower scattering levels, because photons traveling longer paths will be absorbed before being able to escape the medium, depending on the absorption level. Figure 9(b) represents the sensitivity when the speckle phenomenon is not taken in to account. Here, the overall sensitivity decreases with reduced scattering level and absorption. The penetration depth of the light, and its path length, decreases with increasing scattering and absorption, which reduces the probability that light will interact with moving particles. The mean sampling depth [defined by Eq. (8)] is shown in Fig. 10, for the combined effect of speckle and photon penetration depth statistics (shaded symbols) and for the penetration depth statistics alone (closed symbols). The sampling depth decreases with increasing scattering and absorption levels, which is obvious. Accounting for the speckle effect (Fig. 10, shaded symbols) significantly decreases the mean sampling depth. For an absorption coefficient of 0.01 mm^{-1} and $\mu_s'=1.0$ mm^{-1}, the mean sampling depth is reduced from 0.87 to 0.63 mm, whereas when the scattering level is increased to $\mu_s'=4.0$ mm^{-1}, the sampling depth drops from 0.41 to 0.28 mm. This trend is also seen with increasing absorption.

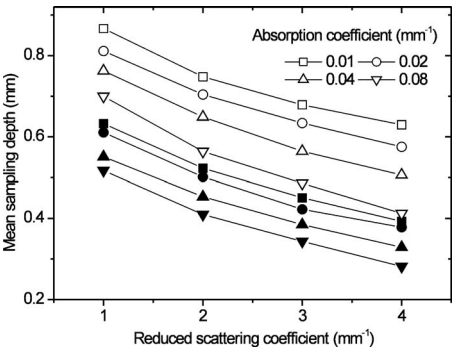

Fig. 10 Mean sampling depth for different scattering levels and absorption levels. Shaded symbols represent the sampling depth with speckle phenomenon taken into account. Closed symbols where the fractional coherence areas (speckles) kept constant ($A_{coh}^{01}=1$).

This shows that the speckle phenomenon is affecting the mean sampling depth, with the relatively strongest effect occurring for the largest scattering coefficient.

4.6 *General Remarks*

In our model, we considered a static turbid matrix with moving particles at a sufficiently low concentration to assume heterodyne detection, hence with a fraction of Doppler-shifted photons $f_1 \ll 1$. For the higher perfusion levels associated with a large concentration of moving scatterers, simplifications such as the linear summation of signals generated at various depths can no longer be applied, since interference between Doppler-shifted light fractions must also be taken into account.

Another aspect that has not been taken into account is the number of times that a detected photon will interact with a certain tissue layer. This will be proportional to the number of crossings of the photon with this layer. Since for detection in reflection mode, this must always be an even number, the probability of multiple crossings will rapidly decay with the number of crossings.

5 Conclusions and Implications

With measurements on two skin locations with largely different absorption and scattering levels, we showed that the signal response (modulation depth of the fluctuating photocurrent) of a laser Doppler perfusion imager using a collimated scanning beam is influenced by tissue optical properties through the speckle phenomenon. We confirmed this with our Monte-Carlo-based theoretical model. Furthermore, we showed that the overall response and the depth sensitivity of the LDPI method are strongly influenced by speckle size changes that occur with changes of tissue optical properties. Due to the speckle phenomenon, the effects of changes in the levels of absorption and scattering on the overall sensitivity can be opposite to those suggested by the photon penetration depth statistics alone, such as illustrated by Figs. 9(a) and 9(b). These findings will help in correctly interpreting the results obtained with a laser Doppler perfusion imager, in particular in situations with a large inhomogeneity of the tissue optical properties.

In real tissue, the depth sensitivity assessment is difficult because discriminating the fraction of detected photons that traveled to certain depths is not possible. Polarization techniques can be considered but an exact estimation of the depth traveled by photons cannot be calculated. An estimation of only the Doppler-shifted fraction of photons can be done by using a polarization filter, but often will result in filtering out singly scattered Doppler-shifted photons, which is preserving its polarization, losing[15] the SNR. The same remarks can be made about low-coherence interferometry,[16] which enables path length discrimination, but without a strong link between the optical path length and the penetration depth of photons. Thus, the depth sensitivity in real tissue was not validated with our model to show the speckle effects. However, the validity of our model, as proven experimentally;[10,17] the effects of speckles on the total sensitivity, as proven in the port-wine stain experiments; and the significance of the predicted effects of speckles on depth sensitivity shown here are evidence that the depth sensitivity is an effect that will occur in real tissue.

Our observations suggest that at certain applications of the perfusion imager special care must be taken to arrive at a conclusion regarding a perfusion change. For example, in burn depth assessment the optical properties of the damaged skin on top of a perfused tissue will play a large role in the instrument sensitivity. Also in interpreting the data obtained with certain drug tests or vasodilatory stimuli where the tissue optical properties can vary rapidly in time and space, care should be taken since both the depth sensitivity and overall response of the instrument can vary independent of perfusion. For instance, a large increase of absorption due to strong vasodilation will lead to a relative overestimation of the perfusion estimation. The shown results help in quantifying combined speckle and photon penetration-depth-related consequences of tissue optical properties for LDPI.

Acknowledgments

This research was sponsored by the Netherlands Technology Foundation STW under Grant No. TTF.5840. R.G. M Kolkman and M. J Mulder are acknowledged for the assistance with photoacoustic measurements.

References

1. H. Fujii, K. Nohira, Y. Yamamoto, H. Ikawa, and T. Ohura, "Evaluation of blood flow by laser speckle image sensing: part 1," *Appl. Opt.* **26**, 5321–5325 (1987).
2. J. D. Briers and S. Webster, "Quasi-real time digital version of single-exposure speckle photography for full-field monitoring of velocity or flow fields," *Opt. Commun.* **116**, 36–42 (1995).
3. T. J. H. Essex and P. O. Byrne, "A laser Doppler scanner for imaging blood flow in skin," *J. Biomed. Eng.* **13**, 189–194 (1991).
4. K. Wårdell, A. Jakobsson, and G. E. Nilsson, "Laser Doppler perfusion imaging by dynamic light scattering," *IEEE Trans. Biomed. Eng.* **40**, 309–316 (1993).
5. D. A. Boas, L. E. Campbell, and A. G. Yodh, "Scattering and imaging with diffusing temporal field correlations," *Phys. Rev. Lett.* **75**, 1855–1858 (1995).
6. J. D. Briers, "Laser Doppler and time-varying speckle: a conciliation," *J. Opt. Soc. Am. A* **13**, 345–350 (1996).
7. V. Rajan, B. Varghese, T. G. van Leeuwen, and W. Steenbergen, "Speckles in laser Doppler perfusion imaging," *Opt. Lett.* **31**, 468–470 (2006).

8. A. Fullerton, B. Rode, and J. Serup, "Skin irritation typing and grading based on laser Doppler perfusion imaging," *Skin Res. Technol.* **8**, 23–31 (2002).
9. E. J. Droog, W. Steenbergen, and F. Sjöberg, "Measurement of depth of burns by laser Doppler perfusion Imaging," *Burns* **27**, 561–568 (2001).
10. V. Rajan, B. Varghese, T. G. van Leeuwen, and W. Steenbergen, "Quantification of spatial intensity correlations and photodetector intensity fluctuations of coherent light reflected from turbid particle suspensions," *Phys. Rev. E* **75**, 060901-4 (2007).
11. R. Bonner and R. Nossal, "Model for laser Doppler measurements of blood flow in tissue," *Appl. Opt.* **20**, 2097–2107 (1981).
12. F. F. M. de Mul, M. H. Koelink, M. L. Kok, P. J. Harmsma, J. Greve, R. Graaff, and J. G. Aarnoudse, "Laser Doppler velocimetry and Monte Carlo simulations on models for blood perfusion in tissue," *Appl. Opt.* **34**, 6595–6611 (1995).
13. R. G. M. Kolkman, E. Hondebrink, W. Steenbergen, T. G. van Leeuwen, and F. F. M. de Mul, "Photoacoustic imaging of blood vessels with a double ring sensor featuring a narrow angular aperture," *J. Biomed. Opt.* **9**, 1327–1335 (2004).
14. L. O. Svaasand, L. T. Norvang, E. J. Fiskerstrand, E. K. S. Stopps, M. W. Berns and J. S. Nelson, "Tissue parameters determining the visual appearance of normal skin and port-wine stains," *Lasers Med. Sci.* **10**, 55–65 (1995).
15. M. G. D. Karlsson and K. Wårdell, "Polarized laser Doppler perfusion imaging—reduction of movement-induced artifacts," *J. Biomed. Opt.* **10**, 064002 (2005).
16. B. Varghese, V. Rajan, T. G. van Leeuwen, and W. Steenbergen, "Path-length-resolved measurements of multiple scattered photons in static and dynamic turbid media using phase-modulated low-coherence interferometry," *J. Biomed. Opt.* **12**, 024020-7 (2007).
17. V. Rajan, B. Varghese, T. G. van Leeuwen, and W. Steenbergen, "Effect of speckles on the depth sensitivity of laser Doppler perfusion imaging," *Opt. Express* **15**, 10911–10919 (2007).